NANO LETTERS
Letter
Cite This: Nano Lett. 2019, 19, 6235−6243
pubs.acs.org/NanoLett

Monolithic Integration of Silicon Nanowire Networks as a Soft Wafer for Highly Stretchable and Transparent Electronics

Taige Dong, Ying Sun, Zhimin Zhu, Xiaoxiang Wu, Junzhuan Wang, Yi Shi, Jun Xu, Kunji Chen, and Linwei Yu*

National Laboratory of Solid State Microstructures/School of Electronics Science and Engineering/Collaborative Innovation Center of Advanced Microstructures, Nanjing University, 210093 Nanjing, China

Supporting Information

ABSTRACT: Assembling nanoscale building blocks into an orderly network with a programmable layout and channel designs represents a critical capability to enable a wide range of stretchable electronics. Here, we demonstrate the growth-in-place integration of silicon nanowire (SiNW) springs into highly stretchable, transparent, and quasicontinuous functional networks with a close to unity interconnection among the discrete electrode joints because of a unique double-lane/double-step guiding edge design. The SiNW networks can be reliably transferred to a soft elastomer substrate, conformally attached to highly curved surfaces, or deployed as self-supporting/movable membranes suspended over voids. A high stretchability of >40% is achieved for the SiNW network on an elastomer, which can be employed as a transparent and semiconducting thin-film material endowed with a high carrier mobility of >50 cm^2/(V s), I_{on}/I_{off} ratio >10^4, and a tunable transmission of >80% over a wide spectrum range. Reversibly stretchable and bendable sensors based on the SiNW network have been successfully demonstrated, where the local strain distribution within the spring network can be directly observed and analyzed by finite element simulations. This SiNW network has a unique potential to eventually establish a new generically purposed waferlike platform for constructing *soft* electronics with Si-based *hard* performances.

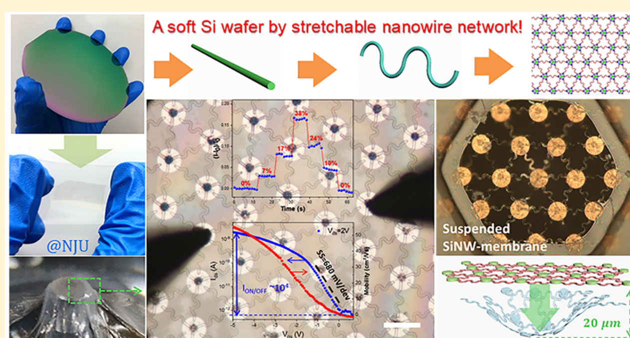

KEYWORDS: *Stretchable electronics, silicon nanowire, nanowire network, sensors, logics*

Soft semiconducting thin-film materials are the basis for constructing a wide range of emerging flexible and wearable logic devices,[1−4] photodetectors,[5,6] flexible displays,[7−9] and artificial skin sensors,[10−12] which are supposed to be deployed over uneven and deformable skin/tissue surfaces and thus demand excellent mechanical flexibility, adaptability, and biocompatibility. For these applications, silicon nanowires (SiNWs) are the most versatile high-quality building blocks, which can be mass-produced via a low-temperature, high-yield, and low-cost fabrication.[13−18] From the view of device applications, assembling these nanoscale building blocks into orderly and programmable networks is a prerequisite. This process is indeed highly challenging but equally rewarding. The synergetic combination of spatial layout and channel geometry design can help to endow c-Si with extra mechanical stretchability—far beyond the limits of bulk materials—while preserving the best-known semiconducting properties of c-Si, such as a high carrier mobility, stability, and well-established doping/passivation controls, which are all highly desired elements for the construction of high-performance *soft* electronics.

Recently, stretchable c-Si spring channels have been demonstrated via geometry engineering by using electron beam lithography (EBL) and etching of the ultrathin monocrystalline Si layer in silicon-on-insulator substrates.[4,19] This development represents a conceptual breakthrough but is also limited by the costly and ineffective manufacturing. In comparison, the self-assembly SiNWs via a vapor−liquid−solid (VLS) mechanism catalyzed by metal droplets[13,20] can also be engineered into sinusoidal spring shapes by using prepatterned guiding channels/pores,[19,21−25] postgrowth buckling by attaching straight SiNWs to a prestrained polymer,[26−28] and by assembling straight Si or metal oxide NWs into a network via solution flow,[29−31] electric field guidance,[15] van der Waals/hydrogen forces,[32] and biorecognition connections.[33] However, the scalable batch-manufacturing and labile integration of an orderly SiNW network, a higher level of assembling capability, has not yet been demonstrated.

In our previous works, an in plane growth of SiNWs has been demonstrated, where low-melting-point droplets of indium (In) absorb a precoated amorphous silicon (a-Si) thin film to produce crystalline SiNWs.[34−36] During the in

Received: June 5, 2019
Revised: August 12, 2019
Published: August 15, 2019

Downloaded via NANJING UNIV on October 27, 2025 at 13:29:28 (UTC).
See https://pubs.acs.org/sharingguidelines for options on how to legitimately share published articles.

ACS Publications © 2019 American Chemical Society

DOI: 10.1021/acs.nanolett.9b02291
Nano Lett. 2019, 19, 6235−6243

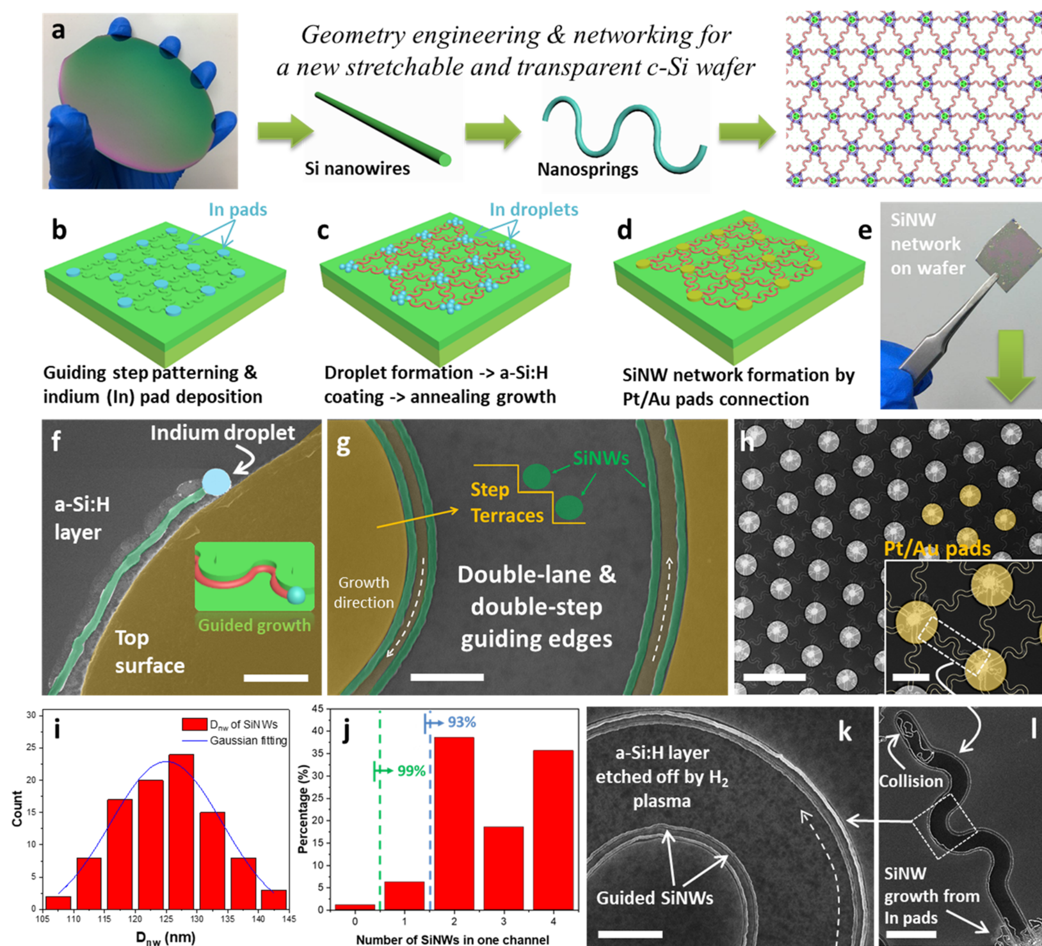

Figure 1. Growth-in-place assembly of the Si nanowire (SiNW) spring network. (a) Schematic illustrations of the evolution of rigid c-Si wafers into a continuous, transparent, and stretchable SiNW spring network. (b−d) Diagrams of the fabrication procedure that involves the patterning of guiding edges and catalyst pads, hydrogenated amorphous Si (a-Si:H) coating as a precursor, annealing for SiNW growth, and Pt/Au electrode pad interconnections, with an image of the final SiNW network on the SiO_2/c-Si wafer shown in part e. (f−h, j−l) SEM images of the guided growth of double-lane SiNWs along the predesigned step edge lines and the network joint by Pt/Au electrode pads, while statistics for the diameters of the SiNWs are provided in part i.

plane solid−liquid−solid (IPSLS) growth, the catalyst droplets can be attracted by simple step edges to produce SiNWs along the edges.[37−43] Built on this capability, we here explore a higher level of monolithic integration of SiNW springs into continuous, stretchable, and semiconducting networks, with a programmable layout and transparency. This process has been enabled by a rather high (close to unity) guided growth and interconnection rate, achieved by a special double-lane and double-step guiding edge design, as well as an optimized network layout. The continuous SiNW networks can be reliably transferred to elastomer thin films, attached to highly curved surfaces, and deployed as self-supported membranes over voids. Together, these critical capabilities highlight the potential of the SiNW network to serve as a solid basis for constructing *soft* electronics with Si-based *hard* performances.

The SiNW networks were grown on a c-Si substrate coated with 300 nm SiO_2, where an array of guiding edges was first patterned. A 2D spring channel and hexagonal network layout, as illustrated schematically in Figure 1a, was formed by using conventional lithography and inductively coupled plasma (ICP) etching of the oxide layer (Figure 1b). At the converging joints of the guiding edges, In pads were deposited and later transformed into discrete droplets via a H_2 plasma treatment in a plasma-enhanced chemical vapor deposition (PECVD) system at 250 °C. Then, a hydrogenated amorphous silicon (a-Si) precursor thin film was coated at 100 °C below the melting point of In (at 157 °C) by a silane plasma, followed by annealing in vacuum at 350 °C to activate the In droplets to absorb the a-Si thin film and leave SiNWs behind (see Figure 1c). Note that once the In droplets touched the nearby guiding edges, the In droplets became attracted to the extra a-Si coated on the vertical-edge sidewalls, and thus, the SiNWs grew along the step edges. After that, the remnant a-Si was selectively etched via a H_2 plasma etching at 150 °C, followed by Au/Pt electrode deposition via lithography and electron beam sputtering to join the SiNW spring channels into a continuous network.

The SiNW network presents a regular hexagonal layout, with a lattice spacing of L_{hex} = 136 μm, where the In catalyst pads are placed at the lattice points and crossed by 3 double-lane guiding channels with 1.5−3 periods of sinusoidal spring design. Ultralong SiNWs, led by the In droplets, grew out of the In pads and followed the guiding step edges (there are two edges in each channel). Figure 1f shows a typical SEM image of a single SiNW grown along a curved step edge and led by an In droplet, which appears brighter in the SEM image. As a

DOI: 10.1021/acs.nanolett.9b02291
Nano Lett. 2019, 19, 6235−6243

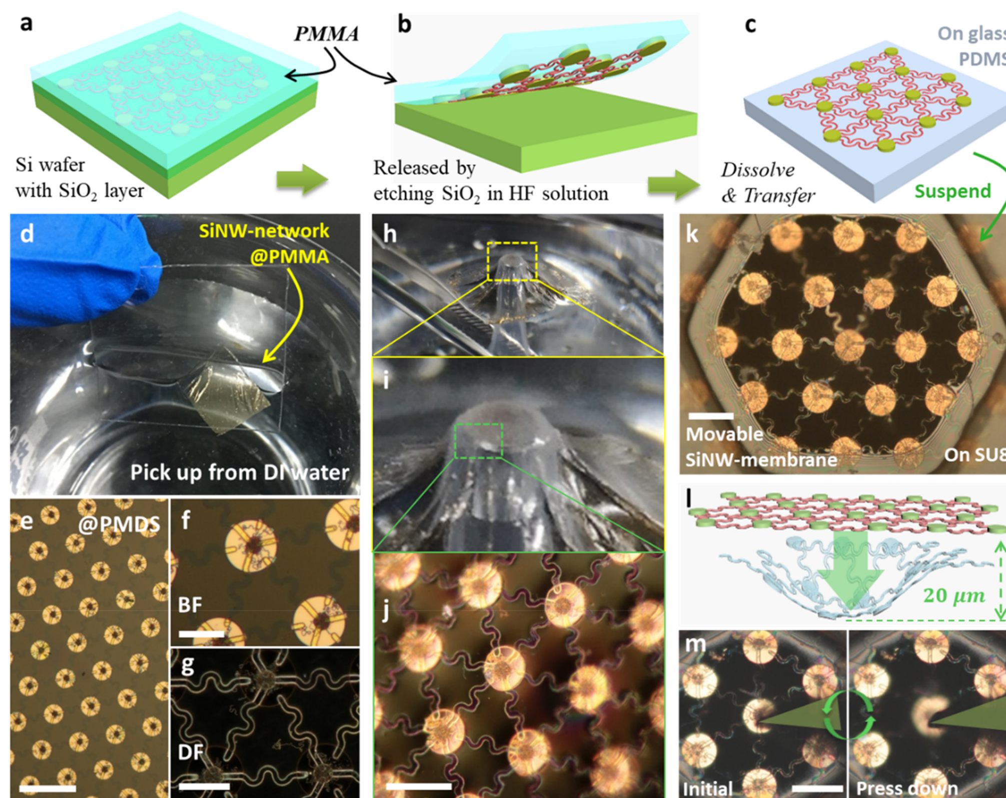

Figure 2. Releasing and transferring the SiNW network. (a−c) Illustrations of coating the PMMA thin film on the sample surface, HF etching to release, and transferring the SiNW network onto soft PDMS or glass substrates. (d) Photo of the picking up of the buoyant SiNW-network@ PMMA thin film from the surface of deionized water, with (e−g) bright-field (BF) and dark-field (DF) microscopic images shown below. (h, i) The soft SiNW-network@PDMS layer attached conformally to the tip of a pointed tube. (j, k) Close examination of the network over the highly curved edge, and continuous and self-sustained suspended SiNW membrane over a void formed in an SU8 thin film. (l, m) Repeatable elastic deformation of the network under downward pressing to a depth of 20 μm.

prerequisite to form a continuous network, there should be at least one continuous SiNW that can travel from one site to its nearest neighbor to establish a bridge for interconnection. After coating the a-Si layer and annealing in vacuum, most of the In droplets can be easily activated to grow, as witnessed in the scanning electron microscope (SEM) image shown in the Supporting Information (SI), Figure S1. For the guiding edges crossing the periphery of the In pads, the local droplets compete for the chance to touch the nearby guided edges, thus, kicking off a guided growth along the predesigned edge lines. Because of the self-avoiding nature of the in plane growth, one step edge can only guide one stable growth of SiNW. The free growth of SiNWs is also observed, as indicated in Figure S1b,c, but the NWs can only travel <5 μm away from the In pads and usually terminate by self-trapping. With proper parameter controls of the step height (h_s), In catalyst droplets (D_{In}), and a-Si layer thickness (h_{aSi}) (see the Experimental Section for more details), basically all the guiding edges can receive one In droplet to produce ultralong SiNWs with a typical length of L_{nw} > 300 μm and a mean diameter of D_{nw} ~ 125 ± 10 nm, as inferred from the statistics shown in Figure 1i.

After the SiNW growth, hollow or filled Au/Pt electrodes 25−34 μm wide were prepared by a lithography, evaporation, and lift-off procedure, to join the SiNW channels into a continuous network. Note that there are two guiding edges in each channel, as marked by the dashed rectangle in Figure 1h, that are separated by 3 μm. These double-lane guiding edges allow the SiNWs to grow from one edge to the end and then to turn back along the opposite edge to the starting In pad, when there is no other guided SiNW present. This feature provides an extra guarantee that the guided growth of SiNWs happening on either side of the double-lane channel will eventually establish a double-link interconnection between neighboring sites. In the meantime, head-to-head collisions can also occur for two SiNWs that randomly grow simultaneously in the same channel but on the opposite guiding edges, and this will lead to the merging and derailing of the leading droplets or occasionally a disruption of the SiNW connection. Fortunately, this collision will most likely happen at the ends of the guiding channels, instead of in the middle, because the catalyst droplets are activated more or less simultaneously and run at similar speeds. Therefore, the SiNWs will meet mostly likely near the far ends of the channels, which will be covered by the Au/Pt metal pads as electric contacts.

To improve the electrical and mechanical interconnection further, a new double-mini-step technology has been adopted here and can produce two or even more ministeps at a single guiding edge to multiply the number of SiNW links, with the same lithography technology. For example, as seen in the SEM image shown in Figure 1g, two ministeps were formed at the guiding edges, which can guide a pair of SiNWs grown in parallel with a narrow separation of only S_{step} = 250 nm. The ministeps can be accomplished via a simple alternating C_4F_8/ O_2 plasma etching procedure, as diagrammed schematically in Figure S2. The photoresistor-coated edges on the SiO_2 layer are first subjected to a C_4F_8 plasma etching to form the first

DOI: 10.1021/acs.nanolett.9b02291
Nano Lett. 2019, 19, 6235−6243

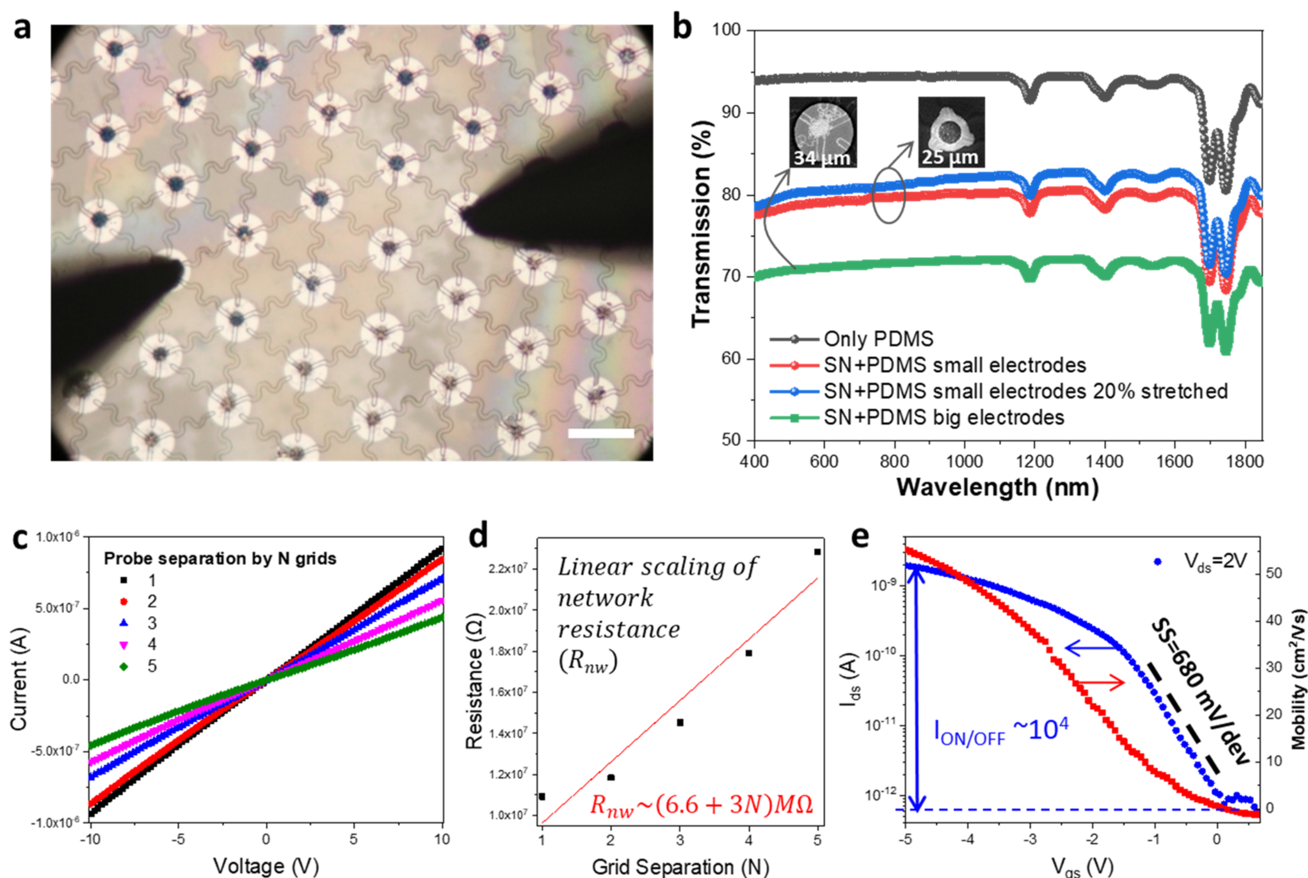

Figure 3. Semiconducting and transparent SiNW network. (a) Microscope image of a SiNW network (SN) on a PDMS substrate, while the transmission spectra of SNs with different electrodes are presented in part b. (c) Current−voltage (I−V) curves measured with different grid separations (N), while the extracted resistances and a linear fit are plotted in part d. (e) Electronic transfer properties of the SiNW spring, measured on a 450 nm SiO_2-coated wafer substrate with a bottom-gate configuration.

ministep, followed by an O_2 plasma etching to erode the edges of the photoresist. This action leaves the plateau of the next ministep, which will be formed in the subsequent C_4F_8 etching cycle. In principle, this alternating etching can be repeated N times to produce N ministeps from a single guiding edge and, thus, N parallel SiNWs. Here, only double-step guiding edges are used, as this has been more than sufficient in view of achieving abundant intersite SiNW connections, while more SiNWs can be readily obtained if required. With all these double-lane and double-step guiding channel designs, the statistics of finding N (from 0 to 4) continuous SiNW connections among the neighboring sites is plotted in Figure 1j according to the SEM observation of 275 different locations. The network connectivity, having at least 1 SiNW link, exceeds >99%, while more than 93% are linked by double SiNWs, thus, providing a solid basis for constructing continuous SiNW networks.

In the next step, a poly(methyl methacrylate) (PMMA) thin film, 100 nm in thickness, was spin-coated over the whole surface (as sketched schematically in Figure 2a), which was immersed in a HF solution to etch the SiO_2 layer underneath and to release the PMMA polymer thin film holding the SiNW network and the joint electrodes together. Then, the PMMA thin film floating on the liquid surface could be picked up and transferred to soft PDMS 200 μm in thickness (as seen in the photo shown in Figure 2d), and after that, the PMMA capping layer was dissolved in acetone, leaving the SiNW network on the PDMS. Figure 2e,f shows the bright-field microscope images of the transferred SiNW network resting on the PDMS, where the good integrity of the whole network, including the metal electrodes and the connecting SiNW channels, can be observed, indicating a high-fidelity transfer process. The transferred SiNW springs are viewed as brighter and color-tinted lines in the dark-field view (Figure 2g), in a strong contrast to the transparent polymer background.

Here, it is noteworthy that, after the in plane growth of SiNWs, there are still many In droplets remaining at the catalyst pads, as seen, for example, in the SEM images shown in Figure S1. However, these regions will be fully covered by larger Pt/Au electrode pads (see Figure 1h). As the Pt/Au electrodes will directly contact and hold the SiNWs grown into the guiding edges, the remnant In pads have basically no influence on the electrical connection between the Pt/Au electrodes and the SiNWs. Moreover, in the following PMMA transfer, the HF solution etching will dissolve not only the underlying SiO_2 layer but also the remnant indium droplets/pads. Therefore, at the end, no In droplets are transferred to the elastomer substrate with the SiNW/electrode network.

The transferred SiNW network can conformally attach to highly curved surfaces, as seen in Figure 2h,i—where a piece of the SiNW network on PMMA is deformed by a tube tip. Closer scrutiny of the contacted area at the top edge (see Figure 2j) reveals that the whole network can easily adapt to curved surfaces, which is a key capability required for deploying stretchable electronics, such as biosensors and photodetectors, over uneven, curved, and impressionable

DOI: 10.1021/acs.nanolett.9b02291
Nano Lett. 2019, 19, 6235−6243

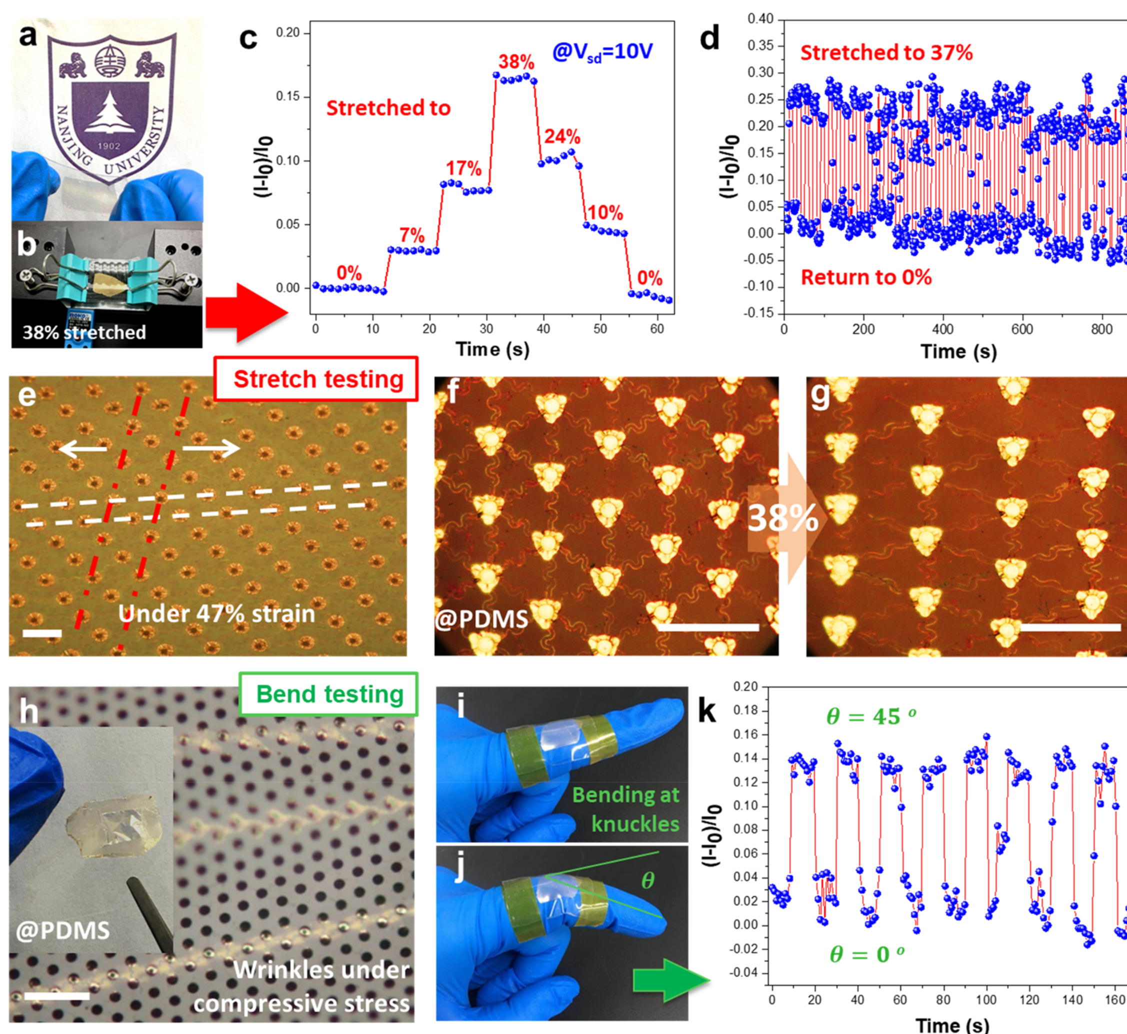

Figure 4. Stretching and bending responses. (a, b) Photos of the stretch testing of a SiNW-network@PDMS thin film by hands and by a pair of clamps. (e) Microscope image of the local deformation of the electrode arrays (with round pads) under stretching in a lateral direction. (f, g) Comparative views of the local deformation of another SiNW spring network (with triangle electrode pads) when subjected to a 38% tensile strain. (c, d) Stepwise stretch and transport current measurement under a constant bias of V_{ds} = 10 V and the change in current under 50 repetitive stretch-release cycles, respectively. (h) Microscope image of the wrinkle formation on the SiNW network under compressive stress, with a photo of the sample on a transparent PDMS thin film. (i, j) Photos of the SiNW network mounted on a finger knuckle for the bend testing, while the recorded current variations at different bending statuses are plotted in part k.

human tissue and retina interfaces.[10,11,44−46] Furthermore, to testify the continuity of the SiNW network, a self-supporting monolayer of the SiNW network has been realized by transferring the network over a hexagonal hole defined in an SU8 layer with a thickness of 20 μm, as seen in Figure 2k. It is remarkable that the suspended SiNW network, consisting of 19 suspended electrodes connected by 44 double-lane SiNW bridges, is completely suspended over a void space of 48 060 μm^2 or ∼220 μm × 220 μm. Note that the obscured SiNW links in the images are due to the vertical displacements, caused by external strains during the dissolving of the PMMA layer and passing the liquid surface, that defocus the SiNW microscope imaging (close examinations confirm that the deviated SiNW links remain continuous).

Thanks to the elastic spring channel design and the continuous layout, the SiNW network by itself can be suspended as a vibrational membrane. For example, in the suspension configuration sketched in Figure 2l, the network membrane can be pressed down by a probe to more than 20 μm deep, with respect to its initial flat level (Figure 2m), and then recover upon release. This pressing-and-releasing test was repeated more than 20 times without causing any breakage or permanent deformation of the suspended network. These observations provide unambiguous proof of the high interconnection rates, excellent robustness, and resilience of the SiNW spring network.

To serve as a generically purposed stretchable *waferlike* semiconducting medium, the optical transmission spectra of the SiNW network resting on PDMS (Figure 3a) are characterized and shown in Figure 3b. The SiNW networks including the opaque metal electrodes, which occupy approximately 22.7% and 14.6% of the surface area of the two electrode diameters of 34 μm and 25 μm, respectively, can achieve a remarkable transmission of 71% and 79% at a 700 nm wavelength (or 72% and 81% at 1300 nm) over a rather wide-ranging spectrum. The transmission dips appearing in the spectra are due to the intrinsic absorptions of the PDMS substrate, which has a transmission of ∼94% in the visible spectrum. For the network with small electrodes, the upper-bound transmission can be estimated to be T_{ub} = 94% × (1 −

DOI: 10.1021/acs.nanolett.9b02291
Nano Lett. 2019, 19, 6235−6243

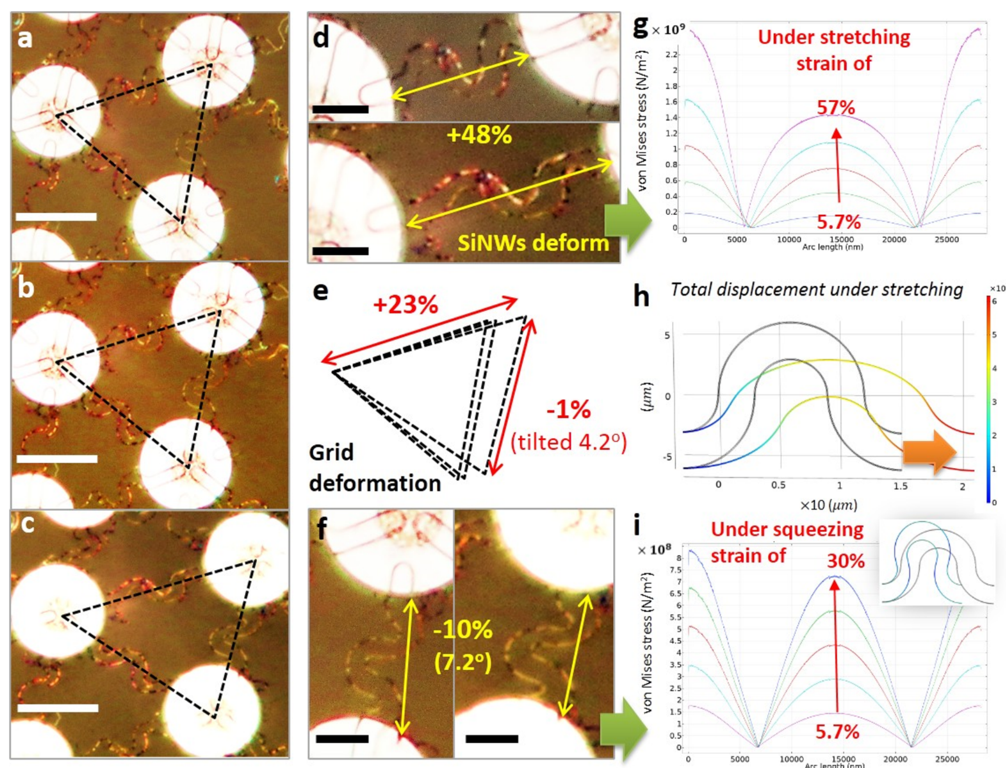

Figure 5. Strain analysis and simulation. (a−c) Microscope images of the local deformation of SiNW-network@PDMS subjected to stretching strains of 0%, 12%, and 23%. (d, e) Direct comparison of the length variations in the SiNW springs after being stretched to 23%, parallel or orthogonal to the stretching direction. (e) Relative electrode site deformations, which can be extracted by overlapping the dashed triangles that join the centers of the three neighbor electrode sites marked in parts a−c. (g, i) The von Mises stress distributions along the top edges of a typical segment of SiNW springs (as shown in part h) for the stretching or squeezing strains are calculated and displayed, respectively.

14.6%) = 80.3%, which is indeed very close to the measured transmission of the SiNW network on the PDMS layer. This result indicates that the SiNW channels by themselves absorb only a tiny portion of the incident light because their average diameter of only 120 nm is small compared to the incident wavelengths.

The electrical properties of the SiNW-network@PDMS have first been characterized by current−voltage ($I-V$) measurements. As shown in Figure 3c, the transport current (or the extracted resistance) decreases (increases) with the grid separation between the electrodes, as measured from N_{grid} = 1−9, implying the good Ohmic contact ensured by the Au/Pt electrodes that join the SiNW channels both mechanically and electrically. This behavior also allows one to treat the network as a quasicontinuous semiconducting thin film with an equivalent grid-separation resistivity of R_{nw} = (6.6 + 3N) MΩ (without an external gating voltage), according to the fit displayed in Figure 3d. To serve as semiconducting channels in field-effect transistors (FETs), a pair of SiNW spring channels 125 μm long were first transferred and placed upon a SiO_2 (450 nm)/c-Si substrate. After removing the PMMA layer by acetone, the spring channels were connected in a bottom-gate configuration. As witnessed in the transfer property shown in Figure 3e, the channel conductivity can be augmented by 4 orders of magnitude at a negative gate bias of V_g = −5V, indicating that the SiNWs are intrinsically p-type doped because of the incorporation of In catalyst atoms into the c-Si matrix, as has been explained in more detail in our previous works.[37,41,47] The SiNW FET achieves a reasonable I_{on}/I_{off} ratio of ~10^4 and a subthreshold swing of 680 mV/dec (though incomparable to the SiNW FETs fabricated with the top-gate configuration in our previous work[41]), and more importantly, the hole carrier mobility in the SiNW spring channels can easily achieve ~50 $cm^2/(V\ s)$, which is indeed significantly higher than their polymer or organic counterparts, typically in the range 10^{-1}−10 $cm^2/(V\ s)$.[48,49]

The electronic transport property of the SiNW-network@PDMS has been further tested at different stretching strains subjected to direct pulling, or more precisely, by using a pair of clamps in a module, for example, as seen in Figure 4a,b. Remarkably, when the network is stretched to more than 40%, as seen in the microscopy picture in Figure 4e, the network grid can easily adapt by elongating in the pulling direction and shrinking in the lateral direction. The deformation is better viewed in the close examination of the SiNW network before and after stretching, as shown in Figure 4f,g, where the SiNW springs remain continuous but deform to be longer in the parallel (and shorter in the normal) directions with respect to the pulling orientation. Meanwhile, the transport current through the SiNW network, measured under a bias of V_{ds} = 10 V with an electrode separation of 55 grids, is also found to be rather sensitive to the stretching strain. As shown in the stepwise stretching-current measurements in Figure 4c, the transport current increases by 17% while being stretched to ~38%, and this variation is well recoverable. Repetitive stretch-release testing for 50 cycles has also been carried out, and the current variations are extracted and plotted in Figure 4d, indicating a reliable pulling strain sensing capability with a gauge factor of g = 82.3. Under compressive strains or squeezing, the SiNW-network@PDMS develops long-wave-

DOI: 10.1021/acs.nanolett.9b02291
Nano Lett. 2019, 19, 6235−6243

Table 1. Summary and Comparison between the SiNW Network Formation Demonstrated Here and Those in the Literature

no.	building blocks	assembly method	network layout	network continuity	stretchable	self-supporting	semiconductor (mobility)	transparency	ref
1	straight oxide or SiNWs	electrostatic field	random crossing	no	no	no	yes (no data)	opaque	60
2	sputtered VLS Si NWs/straight	flow-assisted	random crossing	no	no	no	yes (no data)	opaque	52
3	straight VLS Si NWs	contact-sliding	random crossing	no	no	no	yes (no data)	opaque	61
4	straight Ag/ZnSe NWs	Langmuir–Blodgett	random crossing	no	no	no	yes (no data)	75–95%	62, 63
5	etched random SiNWs	crack masks on SOI	random network	yes	no data	no	yes (no data)	90%	53
6	etched SiNW springs	EBL on SOI	orderly	yes	~100%	yes	yes (no data)	opaque	19, 54
7	straight carbon nanotubes	spin-coating	random network	no	~100%	no	yes (no data)	80–90%	55, 56
8	straight Ag NWs	spin-coating	random network	yes	~50%	no	no	70–85%	57,58
9	straight ZnO nanorods	solvent evaporated assisted	random network	yes	no data	no	1.77 $cm^2/(V\ s)$	71%	59
10	SiNW springs	growth-in-place	regular layout	yes	38% (network) 48% (SiNW)	yes	yes (>50 $cm^2/(V\ s)$)	70–80%	this work

length (~1 mm) wrinkles, as seen in Figure 4h. Furthermore, the bending testing carried out by mounting a piece of the SiNW network sample to the knuckle of a finger (see Figures 4i and 5j, for example) also reveals a robust and repeatable bending strain response, where the transport current increases by 15% at a bending angle of 45°.

It is worthy to note that the soft SiNW channels and the Pt/Au electrode pads in the network are of very different mechanical properties, in terms of stiffness and stretchability. A close investigation of the lattice deformations is shown in Figure 5a–c, where the relative displacement of the electrode pads in the network can be precisely determined by overlapping and comparing their center location triangles (Figure 5e). The overall tensile strain imposed on the network is approximately 23% in the pulling direction, accompanied by a slight squeezing strain of −1% observed in the perpendicular direction. However, at 48%, the local deformation of the SiNW spring links can be considerably larger and almost double the lattice strain (see Figure 5d). The squeezing effect is also far more prominent among the neighboring SiNW springs that are forced to shrink by 10% in terms of the SiNW channel length (Figure 5f). This observation highlights the fact that it is the SiNW springs that absorb all the strain when the network reinforces deformation, which is attributed to the elastic channel design and the hexagonal network formation layout.

To gain further insight into the strain distribution in the SiNW network at different deformations, finite element analysis has been carried out by using COMSOL simulation toolkits. For simplicity, only a very basic unit of the double-lane SiNW spring has been modeled, with the configuration depicted in Figure 5h. The left ports/ends of the SiNWs are fixed while the right ones are subjected to a pulling or pressing displacement of L_{disp} that varies from a compressive strain of −30% to a tensile strain of 57%, approaching to the arc length limit of extension. Figure 5g,i shows the simulated distributions of the von Mises stress along the outer edge lines of the top SiNW springs, under stretching or pressing loads, respectively. The highest stretching stresses are usually found in the segments that have the highest local curvatures in their initial states; here, the absolute stress value is well below 2 GPa (10^9 N/m^2), even under a maximal stretching to 57%, which is also far below the fracture limit of c-Si that is typically ~10 GPa.[50,51] However, at this moment, this model is incapable of addressing the conductivity or resistance variations of the SiNW network under the stretching observed in Figure 4, as the piezoresistivity effects of the SiNW channels are further complicated by the doping, crystallographic orientation, diameter variation, and environmental confinements of the SiNW spring channels. More comprehensive and systematic investigations are definitely required to better understand this phenomenon in the future.

Compared to the previous network formation technologies (see Table 1) that assemble VLS-grown NWs or synthetic building blocks into random cross-linked networks[52] or quasiperiodic arrays with the aid of substrate templates[53] or EBL lithography,[19,54] the growth-in-place deployment of the SiNW networks here indeed represents a far more precise, programmable, and low-cost fabrication strategy. Thanks to the unique elastic channel design and the overall network arrangement, which is rather difficult, if not impossible, to achieve in random networking,[55−63] a highly stretchable, transparent and semiconducting SiNW network can now be batch-manufactured and deployed reliably over soft elastomer substrates, with readily tunable mechanical, electrical, and optical properties according to the needs of specific applications. In addition, a new double-lane and double-step channel design technology ensures an extremely high SiNW connectivity among the network sites. Joined by metal electrode arrays that provide both mechanical and Ohmic electrical connections, a highly adaptive, self-sustainable, and movable SiNW network membrane can be readily fabricated, which has not been possible or demonstrated before.

In summary, the monolithic and programmable growth-in-place integration of a highly stretchable SiNW network has been accomplished, for the first time, via a readily scalable, reliable, and low-temperature batch-manufacturing approach. Thanks to a unique double-lane and double-step channel design and a highly guided growth rate that guarantee a high-quality network interconnection and formation, the continuous SiNW network demonstrates an excellent stretchability of >40%, tunable transmission of >80% on an elastomer substrate, and outstanding semiconducting properties (among stretchable thin-film materials). Stretching and bending sensors have also been demonstrated based on the

DOI: 10.1021/acs.nanolett.9b02291
Nano Lett. 2019, 19, 6235−6243

SiNW/electrode thin film and possess a unique potential to serve as a new type of generic soft wafer technology for constructing various c-Si-based high-performance stretchable electronics and sensors.

Experimental Section. *Guiding Edge Patterning and Double-Mini-Step Formation.* The substrates of Corning glass or c-Si wafers coated with 300−500 nm SiO_2 were cleaned by standard RCA procedures. For the single-step guiding edges, predesigned guiding patterns were defined by conventional lithography and etched 100−150 nm into the SiO_2 layer by using inductively coupled plasma (ICP, Instruments Plasma-Pro System 100). For the double-mini-step guiding edges, after the developing step in the lithography (AZ5214 photoresist), the first ministep of 120 nm deep was formed by an anisotropic C_4F_8 plasma etching, with an RF power, gas flow, and chamber pressure of 400 W, 30 sccm, and 1.8 mTorr, respectively, followed by an O_2 plasma etching with an RF power, gas flow, and chamber pressure of 100 W, 30 sccm, and 10 mTorr, respectively. These treatments eroded/retreated the edges of the photoresist by 200−250 nm laterally. In the next step, the same C_4F_8 etching was carried out again to form the next ministep. Repeating these C_4F_8/O_2 etching cycles for N times can produce N ministeps along the guiding edges, as long as the photoresist layer remains on top.

Catalyst Formation and SiNW Growth. Indium pads (of 30−50 nm thick) located at the lattice points of the hexagonal network and crossing the ends of the guiding edge channels, were deposited and patterned by using lithography, thermal evaporation, and a lift-off procedure. After that, the sample was loaded into the chamber of a PECVD system, where a H_2 plasma treatment was applied at 250 °C, with an 80 sccm flow rate, 120 Pa chamber pressure, and 125 mW/cm^2 RF power density. During this process, the surface oxide layer on the In strips was reduced to allow the In thin film to agglomerate into discrete droplets. Then, the precursor layer of an a-Si thin film was deposited at 150 °C by glow discharge of 10 sccm SiH_4 to a thickness of 40−50 nm with a 30 Pa chamber pressure and 60 mW/cm^2 power density. Upon a simple vacuum annealing at 350−450 °C for 1 h, the In droplets became molten again and moved around laterally to absorb a-Si:H and produce c-SiNWs. During this course, the In droplets that ran into the guiding edge lines were attracted by the extra a-Si layer coated on the vertical-step sidewall to move along and produce SiNWs with a predesigned spring geometry. At the end of the SiNWs, the remnant a-Si layer was selectively etched off by a H_2 plasma etching at 100 °C to preserve only the c-SiNWs.

Metal Electrode Deposition for Network Joining. To join the SiNWs lying in the discrete spring channels into a continuous network, platinum (20 nm)/Au (110 nm) electrode pads 34 or 25 μm wide were defined by lithography and deposited by electron beam evaporation (EBE) to cover the In pads and the ends of the guiding channels (and thus the SiNWs grown within). Prior to the metal evaporation, the native oxide layer on the SiNWs was removed in a 4% HF solution for 20 s.

SiNW Network Formation, Transferring, and Suspension. Prior to network transferring, a 100 nm thick PMMA film was spin-coated on the SiNW network prepared on a Si wafer. Then, the network was released by immersing the sample in a 4% hydrofluoric acid (HF) solution for 1 min to undercut the SiO_2 layer and release the PMMA film that held the network of SiNWs and joining electrode pads. After that, a foreign substrate of a soft PDMS elastomer 200 μm in thickness or a wafer was used to pick up the released and floating PMMA film from the solution. Then, the PMMA film was removed by dissolving in acetone. To demonstrate the self-supported SiNW network, the continuous SiNW network was transferred over the voids or hole spaces defined in the 20 μm thick SU8 photoresist layer. The SiNW network membrane was completely suspended after etching the PMMA layer by using O_2 plasma etching in an RIE system.

Mechanical testing and I−V measurement. The SiNW-network@PDMS thin film was mounted onto a module with two sliding clamps that could hold the thin film at two ends and stretch the sample to a specific displacement controlled by a computer. Electrical connections to the SiNW network were realized by two silver paste electrodes painted directly upon the network and connected through two wire-bonds to a source-monitor unit (Keithley 2636B). During the stretching, a bias was applied between the two electrodes, while the transport current was recorded at room temperature.

■ ASSOCIATED CONTENT

Supporting Information

The Supporting Information is available free of charge on the ACS Publications website at DOI: 10.1021/acs.nano-lett.9b02291.

SEM images of the catalyst formation and SiNW guided growth along step edges and the formation of double-mini-steps along the edge lines by alternative etching (PDF)

■ AUTHOR INFORMATION

Corresponding Author

*E-mail: yulinwei@nju.edu.cn.

ORCID

Linwei Yu: 0000-0002-0801-5210

Notes

The authors declare no competing financial interest.

■ ACKNOWLEDGMENTS

The authors acknowledge the financial support from the National Natural Science Foundation of China under 61674075 and 11874198, the Jiangsu Excellent Young Scholar Program under BK20160020, Jiangsu Shuangchuang Team's Personal Program, and the Fundamental Research Funds for the Central Universities.

■ REFERENCES

(1) Li, G.; Song, E.; Huang, G.; Pan, R.; Guo, Q.; Ma, F.; Zhou, B.; Di, Z.; Mei, Y. *Small* **2018**, *14* (47), 1802985.

(2) Hussain, A. M.; Hussain, M. M. *Adv. Mater.* **2016**, *28* (22), 4219−4249.

(3) Navaraj, W. T.; Gupta, S.; Lorenzelli, L.; Dahiya, R. *Advanced Electronic Materials* **2018**, *4* (4), 1700277.

(4) Cavazos Sepulveda, A. C.; Diaz Cordero, M. S.; Carreño, A. A. A.; Nassar, J. M.; Hussain, M. M. *Appl. Phys. Lett.* **2017**, *110* (13), 134103.

(5) Seo, J. H.; Kan, Z.; Kim, M.; Zhao, D.; Yang, H.; Zhou, W.; Ma, Z. *Adv. Opt. Mater.* **2016**, *4* (1), 120−125.

(6) Li, G.; Song, E.; Huang, G.; Pan, R.; Guo, Q.; Ma, F.; Zhou, B.; Di, Z.; Mei, Y. *Small* **2018**, *14*, 1802985.

(7) Liang, J.; Li, L.; Niu, X.; Yu, Z.; Pei, Q. *Nat. Photonics* **2013**, *7*, 817.

(8) Kim, J.; Shim, H. J.; Yang, J.; Choi, M. K.; Kim, D. C.; Kim, J.; Hyeon, T.; Kim, D.-H. *Adv. Mater.* **2017**, *29* (38), 1700217.

(9) Koo, J. H.; Kim, D. C.; Shim, H. J.; Kim, T.-H.; Kim, D.-H. *Adv. Funct. Mater.* **2018**, *28* (35), 1801834.
(10) Webb, R. C.; Bonifas, A. P.; Behnaz, A.; Zhang, Y.; Yu, K. J.; Cheng, H.; Shi, M.; Bian, Z.; Liu, Z.; Kim, Y.-S.; Yeo, W.-H.; Park, J. S.; Song, J.; Li, Y.; Huang, Y.; Gorbach, A. M.; Rogers, J. A. *Nat. Mater.* **2013**, *12*, 938.
(11) Kim, J.; Kim, M.; Lee, M. S.; Kim, K.; Ji, S.; Kim, Y. T.; Park, J.; Na, K.; Bae, K. H.; Hong, K. K. *Nat. Commun.* **2017**, *8*, 14997.
(12) Hwang, S. W.; Lee, C. H.; Cheng, H.; Jeong, J. W.; Kang, S. K.; Kim, J. H.; Shin, J.; Yang, J.; Liu, Z.; Ameer, G. A. *Nano Lett.* **2015**, *15* (5), 2801.
(13) Schmidt, V.; Wittemann, J. V.; Senz, S.; Gosele, U. *Adv. Mater.* **2009**, *21* (25−26), 2681−2702.
(14) Rurali, R. *Rev. Mod. Phys.* **2010**, *82* (1), 427.
(15) Freer, E. M.; Grachev, O.; Duan, X.; Martin, S.; Stumbo, D. P. *Nat. Nanotechnol.* **2010**, *5* (7), 525−530.
(16) Tsivion, D.; Schvartzman, M.; Popovitz-Biro, R.; von Huth, P.; Joselevich, E. *Science* **2011**, *333* (6045), 1003−1007.
(17) Yuan, G.; Zhao, H.; Liu, X.; Hasanali, Z. S.; Zou, Y.; Levine, A.; Wang, D. *Angew. Chem., Int. Ed.* **2009**, *48* (51), 9680−9684.
(18) Yu, L.; O'Donnell, B.; Alet, P.-J.; Conesa-Boj, S.; Peiro, F.; Arbiol, J.; Roca i Cabarrocas, P. *Nanotechnology* **2009**, *20* (22), 225604.
(19) Rojas, J. P.; Arevalo, A.; Foulds, I. G.; Hussain, M. M. *Appl. Phys. Lett.* **2014**, *105* (15), 154101.
(20) Givargizov, E. I. *J. Cryst. Growth* **1975**, *31*, 20−30.
(21) Kim, J.; Lee, M.; Shim, H. J.; Ghaffari, R.; Cho, H. R.; Son, D.; Jung, Y. H.; Soh, M.; Choi, C.; Jung, S. *Nat. Commun.* **2014**, *5*, 5747.
(22) Shan, Y.; Kalkan, A. K.; Peng, C.-Y.; Fonash, S. J. *Nano Lett.* **2004**, *4* (11), 2085−2089.
(23) Dayen, J. F.; Rumyantseva, A.; Ciornei, C.; Wade, T. L.; Wegrowe, J. E.; Pribat, D.; Cojocaru, C. S. *Appl. Phys. Lett.* **2007**, *90* (17), 173110.
(24) Shan, Y.; Fonash, S. J. *ACS Nano* **2008**, *2* (3), 429−434.
(25) Pevzner, A.; Engel, Y.; Elnathan, R.; Tsukernik, A.; Barkay, Z.; Patolsky, F. *Nano Lett.* **2012**, *12* (1), 7−12.
(26) Khang, D.-Y.; Jiang, H.; Huang, Y.; Rogers, J. A. *Science* **2006**, *311* (5758), 208−212.
(27) Kim, D.-H.; Ahn, J.-H.; Choi, W. M.; Kim, H.-S.; Kim, T.-H.; Song, J.; Huang, Y. Y.; Liu, Z.; Lu, C.; Rogers, J. A. *Science* **2008**, *320* (5875), 507−511.
(28) Jang, K.-I.; Li, K.; Chung, H. U.; Xu, S.; Jung, H. N.; Yang, Y.; Kwak, J. W.; Jung, H. H.; Song, J.; Yang, C. *Nat. Commun.* **2017**, *8*, 15894.
(29) Huang, Y.; Duan, X.; Wei, Q.; Lieber, C. M. *Science* **2001**, *291* (5504), 630−633.
(30) Huang, Y.; Duan, X.; Cui, Y.; Lauhon, L. J.; Kim, K.-H.; Lieber, C. M. *Science* **2001**, *294* (5545), 1313−1317.
(31) Yu, G.; Cao, A.; Lieber, C. M. *Nat. Nanotechnol.* **2007**, *2* (6), 372−377.
(32) Rossi, M.; Fang, W.; Michaelides, A. *J. Phys. Chem. Lett.* **2015**, *6* (21), 4233−4238.
(33) Kovtyukhova, N. I.; Mallouk, T. E. *Chem. - Eur. J.* **2002**, *8* (19), 4354−4363.
(34) Yu, L.; Alet, P.-J.; Picardi, G.; Roca i Cabarrocas, P. *Phys. Rev. Lett.* **2009**, *102* (12), 125501.
(35) Yu, L.; Roca i Cabarrocas, P. *Phys. Rev. B: Condens. Matter Mater. Phys.* **2010**, *81* (8), 085323.
(36) Yu, L.; Roca i Cabarrocas, P. *Phys. Rev. B: Condens. Matter Mater. Phys.* **2009**, *80* (8), 085313−5.
(37) Yu, L.; Chen, W.; O'Donnell, B.; Patriarche, G.; Bouchoule, S.; Pareige, P.; Rogel, R.; Salaun, A. C.; Pichon, L.; Roca i Cabarrocas, P. *Appl. Phys. Lett.* **2011**, *99* (20), 203104−3.
(38) Xu, M.; Xue, Z.; Wang, J.; Zhao, Y.; Duan, Y.; Zhu, G.; Yu, L.; Xu, J.; Wang, J.; Shi, Y.; Kunji, C.; Roca i Cabarrocas, P. *Nano Lett.* **2016**, *16* (12), 7317−7324.
(39) Xue, Z.; Xu, M.; Li, X.; Wang, J.; Jiang, X.; Wei, X.; Yu, L.; Chen, Q.; Wang, J.; Xu, J.; Chen, K.; Roca i Cabarrocas, P. *Adv. Funct. Mater.* **2016**, *26* (29), 5352−5359.
(40) Xue, Z.; Xu, M.; Zhao, Y.; Wang, J.; Jiang, X.; Yu, L.; Wang, J.; Xu, J.; Shi, Y.; Chen, K.; Roca i Cabarrocas, P. *Nat. Commun.* **2016**, *7*, 12836.
(41) Xu, M.; Wang, J.; Xue, Z.; Wang, J.; Feng, P.; Yu, L.; Xu, J.; Shi, Y.; Chen, K.; Roca i Cabarrocas, P. *Nanoscale* **2017**, *9*, 10350.
(42) Xue, Z.; Sun, M.; Dong, T.; Tang, Z.; Zhao, Y.; Wang, J.; Wei, X.; Yu, L.; Chen, Q.; Xu, J.; Shi, Y.; Chen, K.; Roca i Cabarrocas, P. *Nano Lett.* **2017**, *17* (12), 7638−7646.
(43) Xue, Z.; Dong, T.; Zhu, Z.; Zhao, Y.; Sun, Y.; Yu, L. *J. Semicond.* **2018**, *39* (1), 011001.
(44) Hammock, M. L.; Chortos, A.; Tee, B. C.; Tok, J. B.; Bao, Z. *Adv. Mater.* **2013**, *25* (42), 5997−6038.
(45) Kim, D.-H.; Xiao, J.; Song, J.; Huang, Y.; Rogers, J. A. *Adv. Mater.* **2010**, *22* (19), 2108−2124.
(46) Ko, H. C.; Stoykovich, M. P.; Song, J.; Malyarchuk, V.; Choi, W. M.; Yu, C.-J.; Geddes, J. B., Iii; Xiao, J.; Wang, S.; Huang, Y.; Rogers, J. A. *Nature* **2008**, *454*, 748.
(47) Chen, W.; Yu, L.; Misra, S.; Fan, Z.; Pareige, P.; Patriarche, G.; Bouchoule, S.; Cabarrocas, P. R. i. *Nat. Commun.* **2014**, *5*, 4134.
(48) Wang, Y.; Sun, L.; Wang, C.; Yang, F.; Ren, X.; Zhang, X.; Dong, H.; Hu, W. *Chem. Soc. Rev.* **2019**, *48* (6), 1492−1530.
(49) Lee, Y.; Oh, J. Y.; Kim, T. R.; Gu, X.; Kim, Y.; Wang, G. N.; Wu, H. C.; Pfattner, R.; To, J. W. F.; Katsumata, T. *Adv. Mater.* **2018**, *30*, 1704401.
(50) Zhu, Y.; Xu, F.; Qin, Q.; Fung, W. Y.; Lu, W. *Nano Lett.* **2009**, *9* (11), 3934−3939.
(51) O'Mara, W.; Herring, R. B.; Hunt, L. P. *Handbook of semiconductor silicon technology*; Crest Publishing House, 2007.
(52) Lieber, C. M. *MRS Bull.* **2003**, *28* (7), 486−491.
(53) Hossain, M.; Kumar, G. S.; Barimar Prabhava, S. N.; Sheerin, E. D.; McCloskey, D.; Acharya, S.; Rao, K. D. M.; Boland, J. J. *ACS Nano* **2018**, *12* (5), 4727−4735.
(54) Torres Sevilla, G. A.; Qaiser, N.; Corder, M. D.; Shaikh, S. F.; Hussain, M. M. *App. Phys. Lett.* **2018**, *113* (13), 134101.
(55) Chortos, A.; Koleilat, G. I.; Pfattner, R.; Kong, D.; Lin, P.; Nur, R.; Lei, T.; Wang, H.; Liu, N.; Lai, Y. C.; Kim, M. G.; Chung, J. W.; Lee, S.; Bao, Z. *Adv. Mater.* **2016**, *28* (22), 4441−8.
(56) Lee, J.; Lim, M.; Yoon, J.; Kim, M. S.; Choi, B.; Kim, D. M.; Kim, D. H.; Park, I.; Choi, S. J. *ACS Appl. Mater. Interfaces* **2017**, *9* (31), 26279−26285.
(57) Kim, Y.; Jun, S.; Ju, B. K.; Kim, J. W. *ACS Appl. Mater. Interfaces* **2017**, *9* (8), 7505−7514.
(58) Wang, J.; Yan, C.; Kang, W.; Lee, P. S. *Nanoscale* **2014**, *6* (18), 10734−10739.
(59) Park, J. H.; Park, J. H.; Biswas, P.; Kwon do, K.; Han, S. W.; Baik, H. K.; Myoung, J. M. *ACS Appl. Mater. Interfaces* **2016**, *8* (18), 11564−74.
(60) Myung, S.; Lee, M.; Kim, G. T.; Ha, J. S.; Hong, S. *Adv. Mater.* **2005**, *17* (19), 2361−2364.
(61) Yao, J.; Yan, H.; Lieber, C. M. *Nat. Nanotechnol.* **2013**, *8* (5), 329−35.
(62) Acharya, S.; Panda, A. B.; Belman, N.; Efrima, S.; Golan, Y. *Adv. Mater.* **2006**, *18* (2), 210−213.
(63) Liu, J. W.; Wang, J. L.; Wang, Z. H.; Huang, W. R.; Yu, S. H. *Angew. Chem., Int. Ed.* **2014**, *53* (49), 13477−82.

DOI: 10.1021/acs.nanolett.9b02291
Nano Lett. 2019, 19, 6235−6243